GSA - DATA REPOSITORY 2018413

DR1. U-Pb DATING OF CARBONATES BY LA-IC-PMS.

Uranium and Pb isotopic ratios were measured *in situ* on thin sections (30-40µm thick) by LA-ICP-MS at the *Goethe University of Frankfurt (GUF)* using a method similar to that described in Gerdes and Zeh, 2006. The measurement were acquired using a Thermo-Scientific Element 2 ICP-MS, coupled to a RESOlution (Resonetics) 193 nm ArF Excimer laser (CompexPro 102, Coherent) equipped with a S-155 two-volume ablation cell (*Laurin Technic*, Australia). Signal strength at the ICP-MS was tuned for maximum sensitivity while keeping oxide formation below 0.3% (UO/U) and element fraction low (e.g., Th/U = 1). The data were acquired in fully-automated mode overnight in two different analytical sessions. In the first an ablation spot size of 213µm was used and in the second a 313µm spot size. All other parameter and the tuning conditions of the mass spectrometer were kept constant between both sessions. Samples were ablated with a fluence of 0.9 J cm^2 at 8 Hz in a helium atmosphere (0.3 l/min) and mixed in the ablation funnel with 0.9 l/min argon and 0.06 l/min nitrogen. In case of a 213 µm spot this yielded for SRM-NIST614 a depth penetration of about 0.6 µm s-1 and an average sensitivity of 420000 cps/µg g-1 for ^{238}U. The detection limits (4 x background signal) for ^{206}Pb and ^{238}U were ~ 0.1 and 0.03 ppb, respectively. However, at a U signal of less 1000 cps (~ 2 ppb) the data were generally discarded due to enhance scatter on the isotope ratios. Each analysis consisted of 20 s of background acquisition followed by 20 s of sample ablation and 25 s of washouts. During 42 s data acquisition, the signal of ^{206}Pb, ^{207}Pb, ^{232}Th and ^{238}U were detected by peak jumping in pulse counting mode with a total integration time of 0.1 s, resulting in 420 mass scans. Prior to analysis each spot was pre-ablated for 5 s to remove surface contamination.

TABLE DR1. CARBONATE U-Pb AGES AND STABLE ISOTOPE COMPOSITION

Sample name (carbonate phase)	Location				CL response	Age (Ma)*	MSWD†	$^{207}Pb/^{206}Pbi$§	$\delta^{18}O$ (‰, VPDB)#	$\delta^{13}C$ (‰, VPDB)#	Δ_{47} (‰)**	$\delta^{18}O$water (‰)††	TΔ47 (°C)§§
	Borehole	Lat (°N)	Long (°E)	Depth (m)									
RN brachio (shell)	Rigny la Nonneuse	48°24'35"	3°39'41"	1568	non-lumi	**154.2±5.1**	0.8 (26)	0.8297	-2.61±0.79	2.14±0.11	0.658±0.003	1.2	**31±6**
BEBJ2 (micrite)	Baulne en Brie	48°59'16"	3°36'52"	1792	Dull red	**150±16**	2.3 (18)	0.8225	-4.66±0.01	1.37±0.01	0.628±0.011	2.4	**49±5**
VPU9 (micrite)	Villeperdue	48°52'12"	3°32'9"	1892	Dull red	**151.5±6.2**	1.3 (28)	0.8306	-4.54±0.11	1.89±0.04	0.642±0.017	1.5	**43±6**
VPU9 (Cal1)	Villeperdue	48°52'12"	3°32'9"	1892	Bright orange	**120.7±2.2**	0.79 (28)	0.8475	-7.80±0.01	1.81±0.01	0.600±0.025	1.1	**59±10**
VPU8 (Cal1)	Villeperdue	48°52'12"	3°32'9"	1894	Bright orange	**117.5±5.0**	1.1 (23)	0.8444	-7.55±0.01	2.06±0.05	0.597±0.014	2.0	**61±8**
BEBJ8 (Cal1)	Baulne en Brie	48°59'16"	3°36'52"	1788	Bright orange	**118.5±3.6**	1.4 (29)	0.8546	-7.23±0.03	1.18±0.02	0.586±0.004	5.2	**66±5**
FOS1608 (Dol1)	Fossoy	49°2'56"	3°28'55"	1608	non-lumi	**107±13**	1.4 (20)	0.8432	-9.33±0.02	1.75±0.02	0.541±0.001	0.1	**88±7**
RN18 (Cal2)	Rigny la Nonneuse	48°24'35"	3°39'41"	1564	Dull red	**61.1±2.5**	1.5 (25)	0.8707	-16.30±0.05	1.84±0.03	0.564±0.017	-5.4	**76±9**
RN3 (Cal2)	Rigny la Nonneuse	48°24'35"	3°39'41"	1570	Dull red	**68.5±7.7**	1.8 (16)	0.8379	-15.11±0.07	2.2±0.01	0.561±0.003	-4.0	**78±7**
RN3 (Dol2)	Rigny la Nonneuse	48°24'35"	3°39'41"	1570	Bright Red	**37.2±5.3**	1.3 (39)	0.8533	-13.24±0.15	3.20±0.01	0.578±0.003	-6.4	**70±7**

Note:

* Uncertainties on the U-Pb ages are 2σ

† MSWD - Mean Squared Weighted Deviates. The number in bracket is the number of spot analyses made on the sample

§ Isochron intercept on the y-axis is the carbonate initial $^{207}Pb/^{206}Pb$ ratio of the mineralizing fluid.

VPDB - Vienna Pee Dee Belemnite standard.

** Values relative to the 'carbon dioxide equilibrium scale' (CDES), n the 25°C acid digestion scheme (acid fractionation of 0.092‰). Reported uncertainties on Δ_{47} are one standard deviation of the mean (±1 S.D) of replicate measurements (2<n<3) on the same powder

†† Oxygen isotope compositions of mineralizing waters calculated using TΔ47 and the equations of fractionation of oxygen isotopes between the carbonate and water of either O'Neil et al. (1969) for calcite and Horita (2014) for dolomite.

§§Temperatures are computed using the composite Δ47 -T calibration for calcite and dolomite (Eq. 3 from Bonifacie et al., 2017). Uncertainties on TΔ47 are one SE (=S.D. / √n). When the standard deviation of the sample was lower than the long-term standard deviation of the homogeneous standards (average of ±0.018‰, n = 49 in this study), SD of the standards were used to calculate SE for the samples.

Table DR1. Name, location, cathodoluminescence response, U-Pb ages and stable isotopes compositions of the investigated carbonate samples. d ^{13}C, $d^{18}O_{carb}$, $d^{18}O_{water}$ and D_{47} stable isotope data are from Mangenot et al. (2018)

Table DR2. Detailled table on U-Pb elementary composition and geochronology data (samples and standards).

2018413_Table DR2.xlsx

Raw data were corrected offline using a macro-based in-house MS Excel© spreadsheet program. Following background correction, outliers (± 2s) were rejected based on the time-resolved $^{207}Pb/^{206}Pb$ and $^{206}Pb/^{238}U$ ratios together with the Pb and U signal. Due to fast washout, the low volume cell allows to detect inhomogeneity of the ablated material during depth profiling at a level of <0.8µm (<1s). Soda-lime glass SRM-NIST614 was used as a reference glass together with 3 carbonate standards to bracket sample analysis. The $^{207}Pb/^{206}Pb$ ratio was corrected for mass bias (~0.3%) and the $^{206}Pb/^{238}U$ ratio for inter-element fractionation (~9%), including drift over the sequence time, using the SRM-NIST 614.

Correction for sample matrix effects on the $^{238}U/^{206}Pb$ ratio of 3% was made by using a natural calcite spar named WC-1. This natural carbonate is commonly used as reference material for normalization of the $^{238}U/^{206}Pb$ ratio (Li et al., 2014; Coogan et al., 2016; Methner et al., 2016; Roberts and Walker, 2016, Godeau et al. 2018).

The $^{206}Pb/^{238}U$ downhole fractionation during 20s depth profiling was estimate to be 3% based on the common Pb corrected WC-1 analyses, which has been applied as an external correction to all carbonate analyses. Reported uncertainties (2σ) of the $^{206}Pb/^{238}U$ ratio were propagated by quadratic addition of the external reproducibility (2σ) obtained from the SRM-NIST 614 during the analytical session and the within-run precision of each analysis (2 SE; standard error).

Multi-spot analysis (18<n<29) were performed on single carbonate domains previously characterized by cathodoluminescence imaging. Samples were screened before analysis to aim for the highest variability on the $^{238}U/^{206}Pb$ by targeting domains with very low U containing mostly initial common Pb and ones with the highest possible radiogenic Pb component as result of the U decay. U and Pb concentration measured in each ablation spot of the investigated carbonate phases are illustrated in figure DR2.

Analyses plotting along a linear array in the $^{207}Pb/^{206}Pb$ vs $^{208}U/^{206}Pb$ Tera-Wasserburg diagram formed together and the age is defined by the slope of the regression line and the lower intercept with the Concordia. The precision on that age directly depend on the variability of the $^{238}U/^{206}Pb$, the uncertainty on the isotope ratios and the overall statistical fit of the regression line (c.f. MSWD; Brooks et al. 1972).

Repeated analyses (n = 24) of a stromatolitic limestone from the Cambrian-Precambrian boundary in South-Namibia (Feldschuhhorn below Spitskopf formation, Schwarzrand subgroup ; Salor et al. 1996) yielded lower intercept ages of 541.9 ± 5.0 Ma (MSWD = 1.5). This is within uncertainty identical to the U/Pb zircon age of 543 ± 1 Ma from an ash layer of the Spitskopf formation (Bowring et al. 1993). Multiple spots (n = 73) of ASH15 yielded a lower intercept age of 3.067 ± 0.061 (MSWD = 0.99) and an upper intercept of 0.861 for the initial $^{207}Pb/^{206}Pb$. This is identical within uncertainty of the U/Pb age from two labs (3.085 ± 0.044 and 3.005 ± 0.026 Ma ; Vaks et al. 2013) using the conventional U-Pb method. The data of Nama and ASH15 imply an accuracy and repeatability of the method of 1-2% providing the material has sufficient spread in the U/Pb. This is also supported by results of Godeau et al. (2018) where samples analysed in Frankfurt using the same method as described here agreed within uncertainy (+/-1%) with ID solution mode analysis. The analytical data are summarized in table S1 and presented in detail in Supplementary Table S2. Data were plotted in the Tera-Wasserburg diagram (Extended Data) and ages calculated as lower intercepts using Isoplot 3.71 (www.Isoplot.com). All uncertainties are reported at the 2 sigma level.

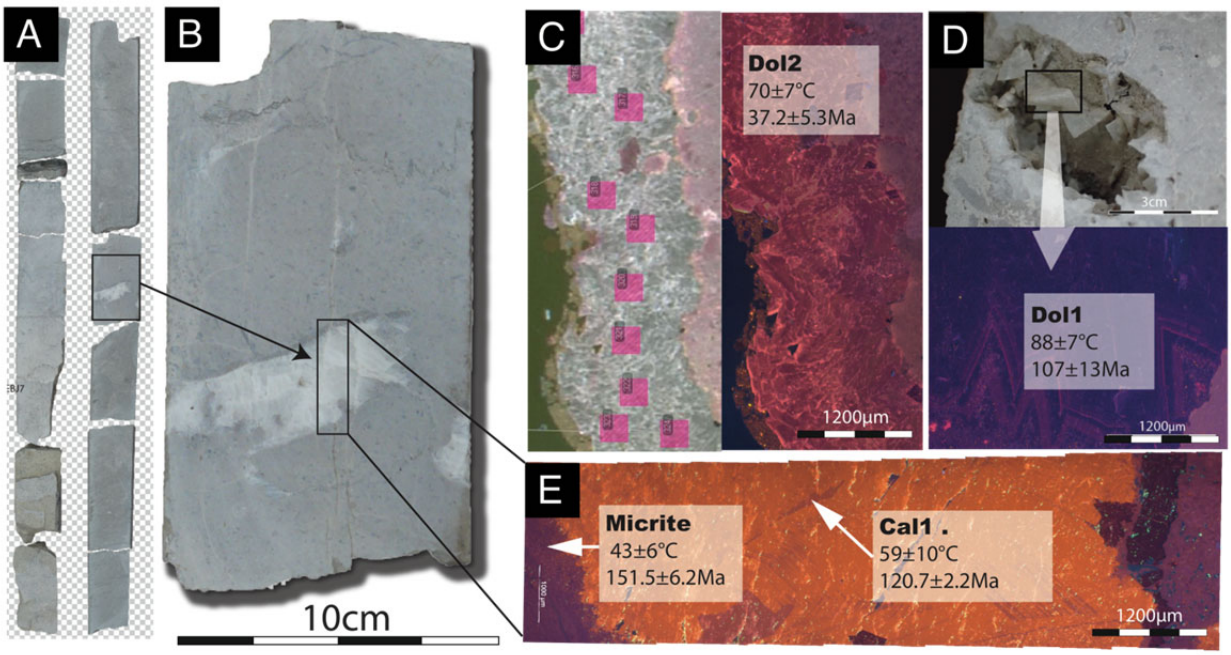

Figure DR1. Petrographic features and thermo-chronology data of some representative samples investigated. A. Macrophotography of a 2m length core interval from the Baulne en Brie well. B. Close-up view of a hand specimen hosting a voluminous pore-filling calcite cement (Cal1) also illustrated in E. C. Thin section microphotography (reflected light and cathodoluminescence) of Dol2 cement with location of some ablation spots where U and Pb isotopes were measured. D. Hand specimen macrophotography and thin section microphotography (cathodoluminescence) of a pore-filling saddle dolomite cement (Dol1) bearing liquid hydrocarbon inclusions (see Mangenot et al. 2018 for more detail). E. Thin section microphotography (cathodoluminescence) showing the host rock micrite and a blocky calcite cement (Cal1).

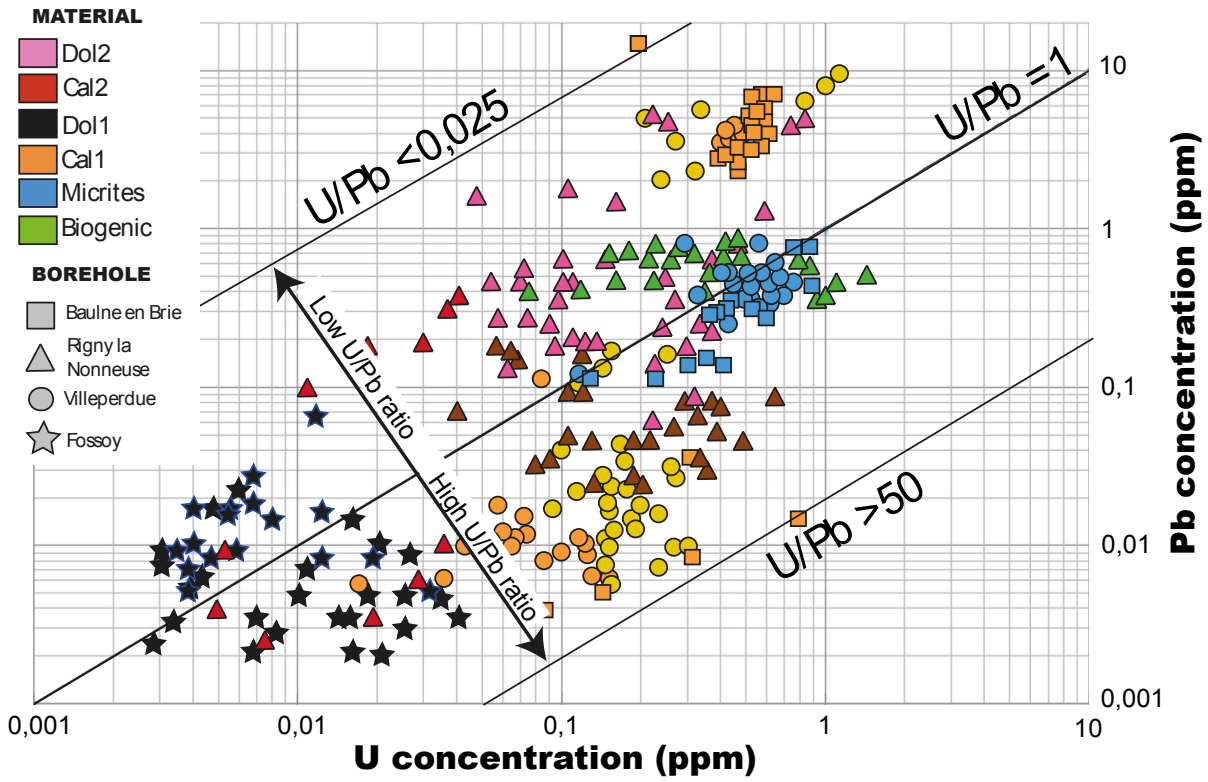

Figure DR2. U and Pb concentration measured in each ablation spot of the investigated carbonate phases. The colors of the symbol refer to specific carbonate phases (from biogenic calcite to Dol2 diagenetic cement) whereas their shape refer to the cores of provenance. Data are provided in table S2.

R.2. DISCUSSION ON "SYN-SEDIMENTARY" CARBONATES

The syn-sedimentary shell and micrite samples formed at the time of the host rock deposition in Middle Jurassic time. However, they record U-Pb ages of 154.2±5.1 Ma, 151.5±6.2 and 150±16 Ma, i.e. younger than the host rock deposition age estimated at 166±2 Ma (Gaumet et al. 1996 and references therein). The Δ_{47} temperatures of these carbonates also indicate abnormally high temperatures (between 31°C and 49°C) compared to expected temperatures for the precipitation of Middle Jurassic marine carbonates at similar latitudes (i.e. 15-27°C; Picard et al. 1998; Lecuyer, 2003). Altogether, the Δ_{47}/(U-Pb) data gathered in this study suggest that these

carbonates experienced recrystallization after deposition, under shallow burial conditions estimated between 100 and 970m (by assuming a geothermal gradient of 35°C/km).

Other petrographic and geochemical arguments confirm this hypothesis, such as the ^{18}O-depleted composition ($\delta^{18}O$ between -2.6 and -4.5‰; Mangenot et al. 2018) compared to marine carbonates precipitated in equilibrium with Middle Jurassic seawater ($\delta^{18}O$ between 1 and -2‰ for Low Magnesium Calcite shells; Veizer et al., 1999) and the observation of petrographic hints for brachiopods pristine layers partial recrystallization.

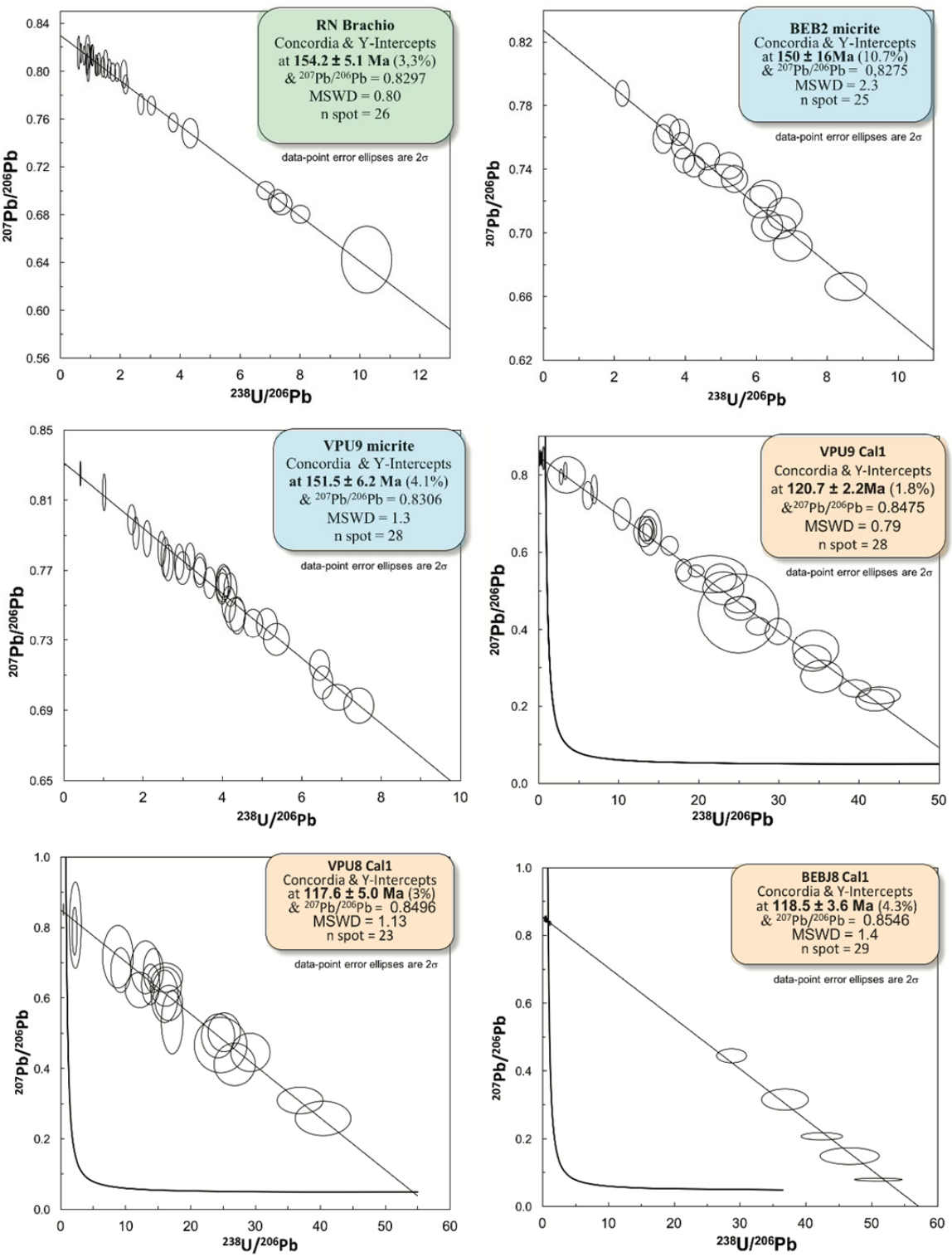
RN Brachio
Concordia & Y-Intercepts
at 154.2 ± 5.1 Ma (3,3%)
& 207Pb/206Pb = 0.8297
MSWD = 0.80
n spot = 26
data-point error ellipses are 2σ
BEB2 micrite
Concordia & Y-Intercepts
at 150 ± 16Ma (10.7%)
& 207Pb/206Pb = 0,8275
MSWD = 2.3
n spot = 25
data-point error ellipses are 2σ
VPU9 micrite
Concordia & Y-Intercepts
at 151.5 ± 6.2 Ma (4.1%)
& 207Pb/206Pb = 0.8306
MSWD = 1.3
n spot = 28
data-point error ellipses are 2σ
VPU9 Cal1
Concordia & Y-Intercepts
at 120.7 ± 2.2Ma (1.8%)
&207Pb/206Pb = 0.8475
MSWD = 0.79
n spot = 28
data-point error ellipses are 2σ
VPU8 Cal1
Concordia & Y-Intercepts
at 117.6 ± 5.0 Ma (3%)
& 207Pb/206Pb = 0.8496
MSWD = 1.13
n spot = 23
data-point error ellipses are 2σ
BEBJ8 Cal1
Concordia & Y-Intercepts
at 118.5 ± 3.6 Ma (4.3%)
& 207Pb/206Pb = 0.8546
MSWD = 1.4
n spot = 29
data-point error ellipses are 2σ
207Pb/206Pb
238U/206Pb

120

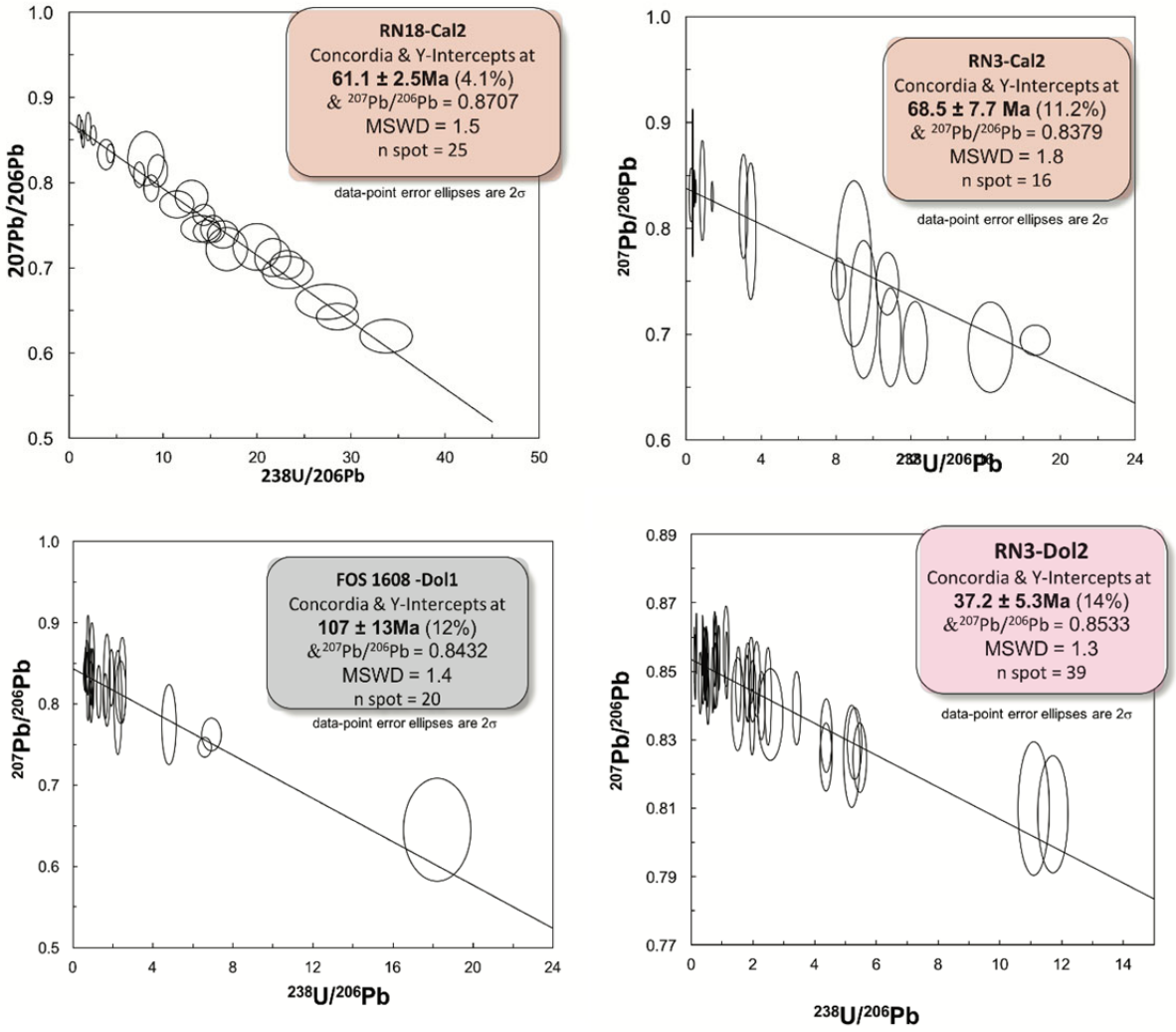

Figure DR3. Tera-Wasserburg diagrams displaying the $^{238}U/^{206}Pb$ *versus* $^{207}Pb/^{206}Pb$ ratios. Samples are ordered from top left to bottom right from oldest to youngest, regardless uncertainty ranges. The different color refers to the sampled carbonate phase: green for brachiopod shell, blue for micrite, orange for Cal1, grey for Dol1, red for Cal2, purple for Dol2.

DR3. EASY Ro% - VITRINITE REFLECTANCE KINETIC MODELING.

In order to evaluate if the newly suggested Δ_{47}/(U-Pb) thermal history would have been identifiable with the conventional vitrinite reflectance thermometer, we performed a calculation of expected EASY Ro% values over time for the two thermal scenario discussed in this study (following the kinetic model of Sweeney and Burham, 1990). As illustrated in figure DR4, modeling results show that the previous thermal history suggested by Uriarte, 1997 (in red on Fig

DR4) and the one newly highlighted by Δ_{47}/U-Pb thermo-chronology (in blue on Fig. DR4) are not prone to generate noticeable discrepancy in Ro% values (by taking into account a typical error of ±0.05% on Ro% measurement). Computed Ro% profiles (Fig. DR4.B) also indicates that both thermal scenarios lead to a value of vitrinite reflectance (0.52 and 0.58 Ro%) that are both indistinguishable with respect the Ro% value measured by Uriatre, 1997 in Callovian shales of the studied area (c.f. 0.6±0.1%Ro - Ambreville borehole – Fig. DR4 and Fig.1 for borehole location). In light of these observations, it is not surprising that the thermal anomaly newly highlighted by the Δ_{47}/(U-Pb) thermo-chronology data would have remained unidentified until today.

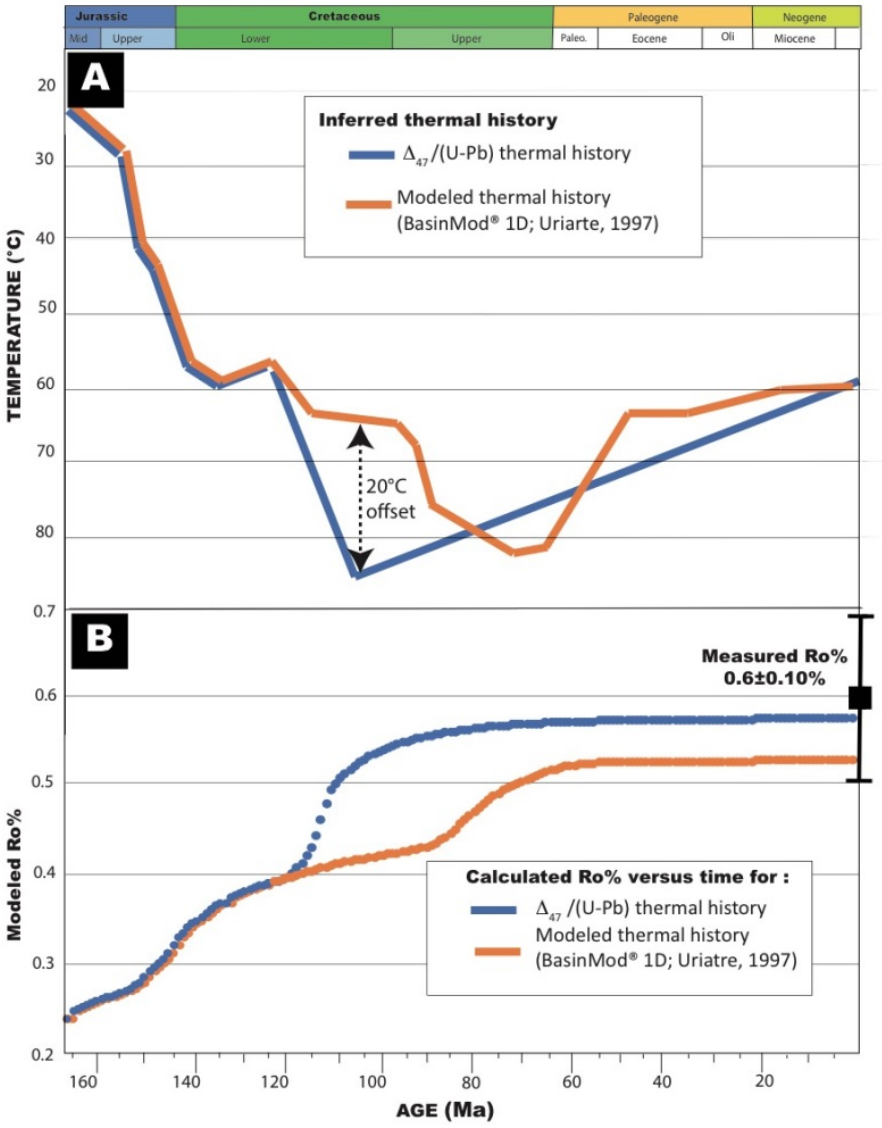

Figure DR4. Calculation of vitrinite reflectance (Ro%) *versus* time for the two thermal histories illustrated in panel A with blue and orange dashed lines. Panel B illustrate the calculation of Ro% *versus* time based on the EASY % Ro kinetic model of Sweeney and Burham (1990), which use the time-temperature history (long dashed line) of the two thermal history reported in panel A. The values of Ro% measured at present day by Uriarte (1997) in the Upper Callovian shales (0.6±0.1% ; Ambreville well on Fig. 2) is also reported with a black square on panel B.

REFERENCES CITED IN THE DATA REPOSITORY

Bowring, S. A., Grotzinger, J.P., Isachsen, C.E., Knoll, A.H., Pelechaty, S.M. and Kolosov, P., 1993, Calibrating rates of Early Cambrian evolution : Science, v.261, p.1293-1298. http://doi.org/10.1126/science.11539488

Brooks, C., I. Wendt, and S. R. Hart, 1972, Realistic use of 2-error regression treatments as applied to rubidium-strontium data : Rev. Geophys., v.10, p. 551–577, http://doi.org/10.1029/RG010i002p00551

Coogan, L.A., Parrish, R.R., and Roberts, N.M.W., 2016, Early hydrothermal carbon uptake by the upper oceanic crust: Insight from in situ U-Pb dating: Geology, v. 44, p. 147–150, http://doi.org/10.1130/G37212.1

Gaumet, F., Garcia, J.P., Dromart, G., and Sambet, G., 1996, Contrôle stratigraphique des faciès, géométries et profils de dépôt de la plate-forme carbonatée bourguignonne au Bathonien-Callovien : Bull. Soc. Géol. Fr., v. 167, p. 409-421, http://doi.org/10.1007/978-3-642-78849-9_5

Gerdes, A., and Zeh, A., 2009, Zircon formation versus zircon alteration — New insights from combined U–Pb and Lu–Hf in-situ LA-ICP-MS analyses, and consequences for the interpretation of Archean zircon from the Central Zone of the Limpopo Belt: Chemical Geology, v. 261, p. 230-243. https://doi.org/10.1016/j.chemgeo.2008.03.005

Godeau, N., Deschamps, P., Guihou, A., Leonide, P., Tendil, A., Gerdes, A., Hamelin, B., and Girard, J.P., 2018, U-Pb dating of calcite cement and diagenetic history in microporous carbonate reservoirs: Case of the Urgonian Limestone, France : Geology, v. 46, p. 247–250, http://doi.org/10.1130/G39905.1

Lecuyer, C., 2003, Thermal evolution of Tethyan surface waters during the Middle-Late Jurassic: evidence from $\delta^{18}O$ values of marine fish teeth : Paleoceanography, v.18, p.1076, http://doi.org/10.1029/2002PA000863

Li, Q., Parrish, R.R., Horstwood, M.S., and McArthur, J.M., 2014, U–Pb dating of cements in Mesozoic ammonites: Chem. Geol., v. 376, p. 76–83, http://doi.org/10.1016/j.chemgeo.2014.03.020

Mangenot, X., Gasparrini, M., Rouchon, V., and Bonifacie, M., 2018, Basin scale thermal and fluid-flow histories revealed by carbonate clumped isotopes Δ_{47} - Middle Jurassic of the Paris Basin: Sedimentology, v. 65, p. 123-150, http://doi.org/10.1111/sed.12427

Methner, K., Mulch, A., Fiebig, J., Wacker, U., Gerdes, A., Graham, S.A., and Chamberlain, C.P., 2016, Rapid Middle Eocene temperature change in western North America : Earth Planet. Sci. Lett., v. 450, p. 132–139, http://doi.org/10.1111/sed.12427

Picard, S., Garcia, J.P., Lecuyer, C., Sheppard, S.M.F., Cappetta, H., and Emig, C.C., 1998, $\delta^{18}O$ values of coexisting brachiopods and fish: temperature differences and estimates of paleo-water depths: Geology, v. 26, p. 975–978, http://doi.org/10.1130/0091-7613(1998)026<0975:OVOCBA>2.3.CO;2

Roberts, N. M. W., Rasbury, E. T., Parrish, R. R., Smith, C. J., Horstwood, M. S. A., and Condon, D. J., 2017, A calcite reference material for LA-ICP-MS U-Pb geochronology: Geochemistry, Geophysics, Geosystems, http://doi.org/10.1002/2016GC006784

Roberts, N.M.W., and Walker, R.J., 2016, U-Pb geochronology of calcite-mineralized faults: Absolute timing of rift-related fault events on the northeast Atlantic margin: Geology, v. 44, p. 531–534, http://doi.org/10.1130/G37868.1

Saylor, Z. and Grotzinger, J. P. 1996, Reconstruction of important Proterozoic-Cambrian boundary exposures through the recognition of thrust deformation in the Nama Group of southern Namibia, Communs geol. Surv. Namibia, v.11, p.1–12.

Sweeney, J.J., and Burnham, A.K., 1990, Evaluation of a simple model of vitrinite reflectance based on Chemical kinetics: AAPG bulletin, v. 74, p. 1559-1570

Uriarte, J. 1997, Maturité thermique des sédiments de la bordure sud-est du Bassin de Paris [*PhD thesis*] : *University of Geneva*, 146 p.

Vaks, A. et al. 2013, Pliocene–Pleistocene climate of the northern margin of Saharan–Arabian Desert recorded in speleothems from the Negev Desert, Israel : Earth and Planetary Science Letters, v.368, p.88–100. http://doi.org/10.1016/j.epsl.2013.02.027

Veizer, J., Ala, D., Azmy, K., Bruckschen, P., and Buhl, D., 1999, $^{87}Sr/^{86}Sr$, $\delta^{13}C$ and $\delta^{18}O$ evolution of Phanerozoic seawater: Chem. Geol., v. 161, p. 59–88. http://doi.org/10.1016/S0009-2541(99)00081-9